International journal of COMADEM
Vol # No # (January 2022) p.##-##

COMADEM

International Journal of Condition Monitoring and Diagnostic Engineering Management

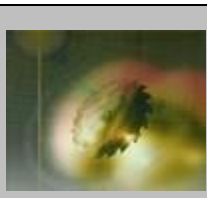

Study the effect of obstacle arrangements on the dam-break flow

Alireza Khoshkonesh 1[a] *, Taimoor Asim 2[b], Rakesh Mishra 3[c], Fariba Ahmadi Dehrashid 4[a] *, Payam Heidarian 5[d], and Blaise Nsom 6[e]

[a] *Department of Water Science and Engineering, University of Bu Ali Sina, 65178 Hamedan, Iran*
[b] *Robert Gordon University, Garthdee Roa, AB10 7GJ ABERDEEN, United Kingdom*
[c] *School of Computing and Engineering University of Huddersfield, HD1 3DH HUDDERSFIELD, United Kingdom*
[d] *MSc in water and hydraulic structures engineering, Department of hydraulic structures, Faculty of civil and environment engineering, Tarbiat Modares University, Iran*
[e] *Université de Bretagne Occidentale. IRDL/UBO UMR CNRS 6027. Rue de Kergoat, 29285 Brest, France*

∗ *Corresponding author. Tel.: +98-912-496-3632; email: alirezakhshknsh42@gmail.com*

ABSTRACT

Infrastructure, including roads, bridges, and municipal facilities, act as barriers to the downstream propagation of flood waves following a dam failure. The aim of this work is to investigate the effects of the obstacles and their arrangement on the evolution of flood waves during a dam breach using a numerical approach. The obstacles were arranged in two arrangements (triangular and inverted triangular) perpendicular to the flow direction in the downstream channel. Wave propagation during dam failure and flow dynamics were modelled by the finite volume method (FVM) using a CFD package. The evolution of the free surface of the dam breach was traced using the volume of fluid (VOF) method. However, the uncertainty of the model was evaluated using a sensitivity analysis with respect to the mesh resolution and turbulence models. The turbulence characteristics were captured by large-eddy simulations (LES) after validating the model using experimental data from the literature. The results show that the model can efficiently reproduce the wave development during a dam failure and the flow characteristics. The arrangement of the obstructions played an important role in the development of flow around the obstructions through the downstream channel. In this direction, the transitional flow regime, resultant forces in reservoir, and three-dimensional flow velocity around the obstacles were predicted for different arrangements.

Keywords: *Dam-break, obstacles, arrangement, FVM, VOF, LES.*
Article history: *Received ; Published .*

Nomenclature

a1, a2: distance between neighbor obstacles

d_0: mean size of the mesh cells

t: time after the dam-break wave formation

x: the overall channel length

D, D_w: dam-break flow depth

F_p: Resultant value of the pressure forces

Fr: Froude number of the dam-break flow

F_s: Resultant value of the shear forces

H_0, H_{w0}: Initial depth of the water column inside the reservoir

H, $H(x,t)$: Dam-break free surface height at the points of x and time of t

L_i: Length of the downstream channel in distance i

L_r: Length of the reservoir

L_t: Total length of the reservoir

Q: Inlet or outlet flow rate from a mesh block

T1: Triangular arrangement of obstacles

T2: Reverse triangular arrangement of obstacles

W_r: Width of the reservoir

1. Introduction

Infrastructures, including buildings, roads, and bridges, play an important role in dissipating flood energy. This is because these structures act as vertical barriers against the propagation of flood waves. Catastrophic floods triggered by dam failures around the world have cost many lives and property in recent decades. Many urban areas downstream of the dams are affected by the severe flood events. In experimental and numerical studies dealing with the dam breach phenomenon, the resistance effect of infrastructures against flood development is an interesting topic.

When a dam breaks, the still water column in a reservoir collapses and rapid unsteady flow occurs in the downstream channel. Both reservoir and downstream conditions can affect the propagation of flood waves during a dam breach. Reservoir conditions, including water level, gradient, fluid viscosity, and shape of the reservoir, are important parameters for the generation and evolution of the flood wave during a dam failure, especially in the initial phase (Nsom et al. (2000-2019), Khoshkonesh et al. (2019,2021), Bahmanpouri et al. (2020)). The conditions in the downstream channel, including tailwater depth, floodplain, transitions or obstructions, and complex geometry, can alter the flow characteristics of the dam breach as well (Kocaman and Guzel (2011), Yilmaz et al. (2013), Aureli et al. (2015), Gu et al. (2017), Khoshkonesh et al. (2019), English et al. (2021), Ahadiyan et al. (2022)).

The complex geometry in the downstream channel leads to the reflection of the dam break wave, the formation of jumps and local 3D flows, oblique waves and flow detachments (Ozmen-Cagatay and Kocaman (2010), Ozmen-Cagatay and Kocaman (2012), Kocaman and Ozmen-Cagatay (2012), Oertel et al. (2012), Azimi et al. (2018)). The single or series of obstructions, the invert hump and the lateral transitions in the downstream channel form a complex geometry that leads to the development of a mixed flow regime and dissipation of the energy of the dam failure (Soares-Frazao and Zech (2008), Wu et al. (2013), Yilmaz et al. (2017), Yu et al. (2019)).

There are numerous studies, both experimental and numerical approaches, on the effect of isolated or arrayed obstacles on the propagation of flow during dam failure in the downstream channel (Soares-Frazao and Zech (2007), Hansch et al. (2014), Issakhov et al. (2018), Issakhov and Imanberdiyeva (2019), Saghi and Lakzian (2019), Issakhov and Zhandaulet (2020)).

However, the resistance of a group of obstacles downstream of the dam to the propagation of dam failure waves has been investigated in only a few studies (Soares-Frazao and Zech (2008), Saleh et al. (2019), Fan et al. (2020)). Moreover, the arrangement of obstacles has not been considered as a crucial factor in the development of rotational flow, air entrapment, three-dimensional velocities and specific flow energy in the literature. However, this is crucial especially in urban and residential areas due to the different arrangement of buildings, roads and other infrastructures in cities.

Therefore, in the present study, wave propagation during a dam failure with a group of obstacles was simulated in two triangular and inverted triangular arrangements using a CFD package Flow-3D. The 3D numerical model was used in both simulations, while the Navier-Stokes equations were discretized using the second-order finite volume method and the explicit central difference schemes. The evolution of the free surface was followed using the volume of fluid (VOF) advection. The model was validated using the experimental data published in the literature. Accordingly, the model uncertainty was evaluated by sensitivity analysis of the mesh resolution and turbulence models. The model of large-eddy simulations (LES) was adopted for both arrangement cases after the validation tests.

2. Material and Methods

2.1. Governing equations

The Navier-Stokes equations of motion in three-dimensional Cartesian coordinates and the addition of the volume and area components are given in equations (1-4).

$$\frac{\partial(uA_x)}{\partial x}+\frac{\partial(vA_y)}{\partial y}+\frac{\partial(wA_z)}{\partial z}=0 \tag{1}$$

$$\frac{\partial u}{\partial t}+\frac{1}{V_f}\left(uA_x\frac{\partial u}{\partial x}+vA_y\frac{\partial u}{\partial y}+wA_z\frac{\partial u}{\partial z}\right)= -\frac{V_f}{\rho}\left(\frac{\partial p}{\partial x}\right)+\frac{\mu}{\rho}\left(\frac{\partial^2(A_xu)}{\partial x^2}+\frac{\partial^2(A_yu)}{\partial y^2}+\frac{\partial^2(A_zu)}{\partial z^2}\right)+g_x \tag{2}$$

$$\frac{\partial v}{\partial t}+\frac{1}{V_f}\left(uA_x\frac{\partial v}{\partial x}+vA_y\frac{\partial v}{\partial y}+wA_z\frac{\partial v}{\partial z}\right)= -\frac{V_f}{\rho}\left(\frac{\partial p}{\partial y}\right)+\frac{\mu}{\rho}\left(\frac{\partial^2(A_xv)}{\partial x^2}+\frac{\partial^2(A_yv)}{\partial y^2}+\frac{\partial^2(A_zv)}{\partial z^2}\right)+g_y \tag{3}$$

$$\frac{\partial w}{\partial t}+\frac{1}{V_f}\left(uA_x\frac{\partial w}{\partial x}+vA_y\frac{\partial w}{\partial y}+wA_z\frac{\partial w}{\partial z}\right)= -\frac{V_f}{\rho}\left(\frac{\partial p}{\partial z}\right)+\frac{\mu}{\rho}\left(\frac{\partial^2(A_xw)}{\partial x^2}+\frac{\partial^2(A_yw)}{\partial y^2}+\frac{\partial^2(A_zw)}{\partial z^2}\right)+g_y \tag{4}$$

V_f, A_x, A_y *and* A_z, are volume and area fractions in *x, y* and *z* directions. Also, $u, v, w, p, v, \rho, g_x, g_y$ and g_z denote the velocity components, fluid pressure, kinematic viscosity, fluid density and body accelerations. The volume of fluid method is used to track the evolution of the free surface area of the dam break across the channel. In addition, *F* represents the cells that contain the fluid. The *F* values are equal to 1 and 0 in fluid-filled and empty cells, respectively. The *F* value is a number between zero and one in half-filled cells (Hirt and Nichols (1981), Flow Science (2012)).

2.2. Initial and boundary conditions

The dimensions of the model and the initial and boundary conditions are shown in Figures 1 and 2 and Table 1. The computational domain included the four mesh blocks (Fig. 2). The free surface was a slip-free boundary condition, while the shear stresses at the free surface were zero.

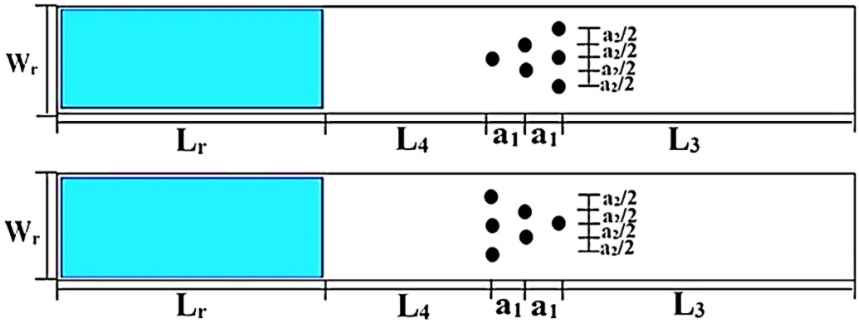

Figure 1. The plan of the dam-break models in triangular (up), and reverse-triangular (down) arrangements

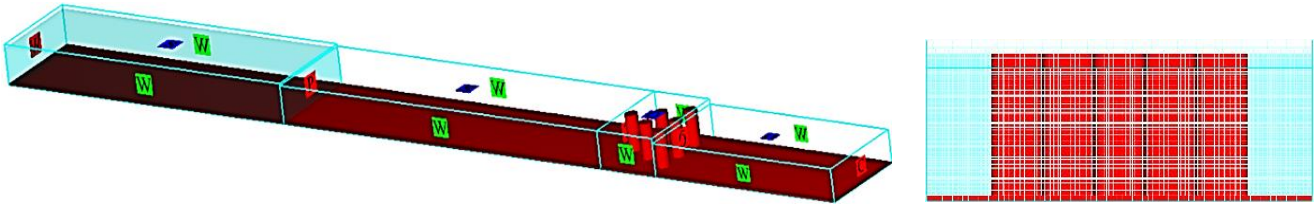

Figure 2. The initial and boundary conditions (left), and the mesh resolution in the obstacles' cross-section (right) in triangular arrangement

The wall boundary condition was applied to the channel bottom, left, and side walls. The stag pressure condition set fluid velocities in the reservoir upstream to zero. The water depth of the reservoir H_{w0} represented the initial condition. In this study, the size of the computational domain in both cases was 15*1.5*0.5m^3 in x*y*z direction. The calculation areas were covered by a structured mesh. The end point of the downstream channel was an outlet. In addition, all obstacles were oriented in the direction of the downstream channel.

Table 1. Dimensions of the dam-break models according to figure 1

models	$H_0(m)$	$a_2(m)$	$a_1(m)$	$W_r(m)$	$L_4(m)$	$L_3(m)$	$L_r(m)$	$Lt(m)$
Triangular T1	0.5	0.4	0.5	1.5	5.76	3.24	5	15
Reverse-triangular T2	0.5	0.4	0.5	1.5	5.76	3.24	5	15

3. Results and Discussion

The model was validated using the experimental data reported by Fraccarollo and Toro (1995), Lobovsky et al. (2014), Liu and Liu (2017). Sensitivity analysis was performed with respect to grid resolution and turbulence model as shown in Fig. 3-5. The model underestimated the temporal variation of the flow depth of the dam breach at the control point of x =72.2cm, downstream the dam site (Fraccarollo and Toro (1995). Accordingly, the x-axis represents the duration of the dam break experiment from the beginning of the collapse of the water column to the wave development across the downstream. In addition, the y-axis shows the flow depth of the dam break at the control point of x =72.2cm. However, the grid resolution and turbulence model did not significantly affect the model accuracy. In fact, the NRMSE value was about 10.9% for all models. As can be seen in Fig. 3, all models underestimated the flow depth by about 1.5 cm during t = 1s to t = 4s.

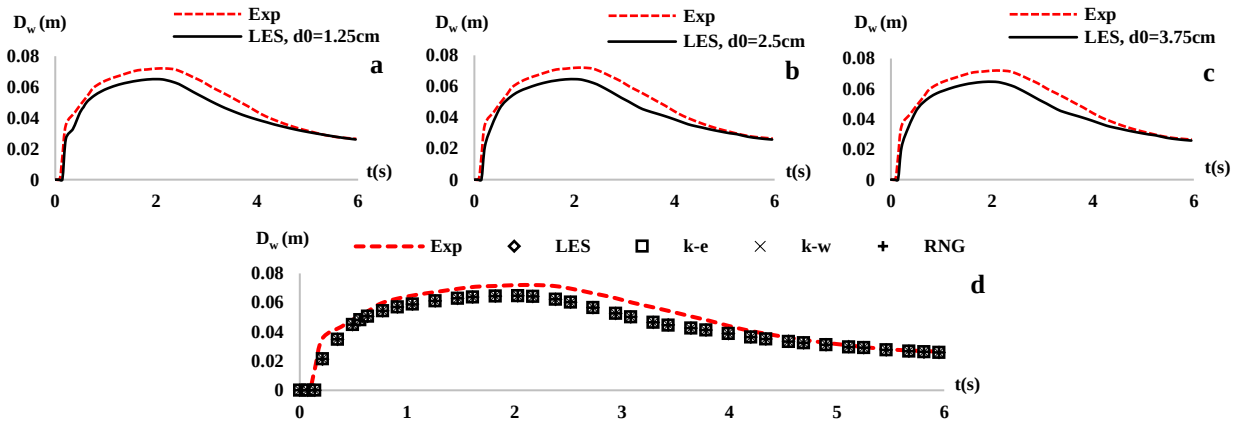

Figure 3. Temporal variation of the dam-break flow depth D_w in the near field, (a-c) sensitivity analysis results on mesh resolution, (d) on turbulence models

Model accuracy in predicting the temporal variation of flow depth was reduced by decreasing the mesh resolution. The accuracy of the model in predicting the temporal variation of flow depth was reduced at the dam site (x=0) by decreasing the mesh resolution from d_0 = 2.5cm to d_0 = 3.75cm (Fig. 4). An evenness appeared in the diagram (Fig. 4c). The reason for this was that the discretization of the equations of motion in larger cells increased the error in the interpolation of the momentum values in the computational domain. It is worth noting that the performance of the model was much higher at a distance than near the reservoir. Moreover, the turbulence models did not play such an important role in the accuracy of the model as in the first case (Fig. 4). The model also showed high accuracy in predicting the evolution of the free surface during dam failure at all stages except the middle stage. It overestimated the height of the free surface by reducing the mesh resolution. The results show that the mesh resolution has a greater influence on the model accuracy compared to the turbulence models. LES model used in both simulations of the obstacle array in the downstream channel. The accuracy of the model in reproducing the evolution of the dam-free surface was examined using the normal root mean square error (NRMSE).

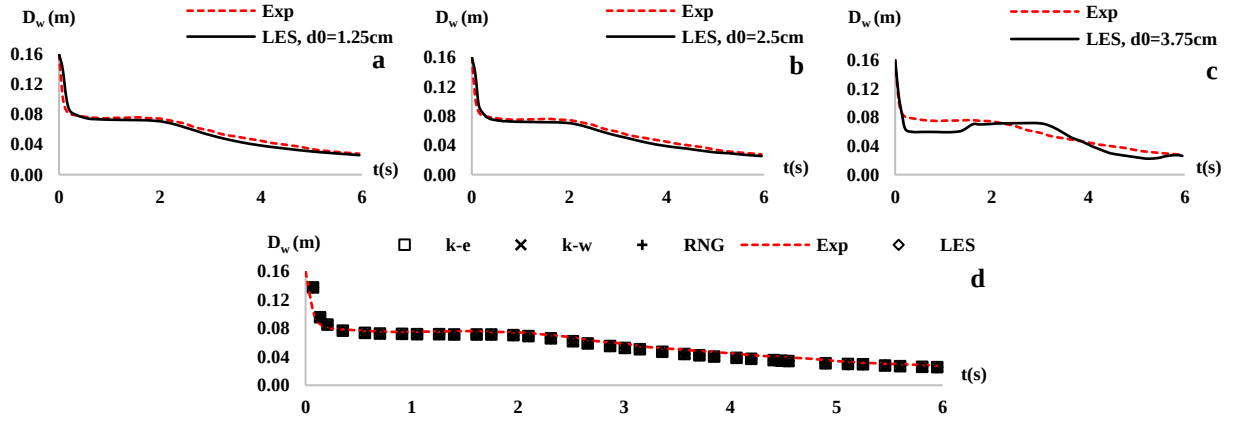

Figure 4. Temporal variation of the dam-break flow depth D_w in the dam site (a-c) sensitivity analysis results on mesh resolution, (d) on turbulence models

Table 2. Dam-break simulation features (validation with experimental results of Lobovsky et al. 2014)

Model	Run time (h)	Mesh cells mean diameter (cm)	Total number of cells in mesh block1 in *x*y*z* direction	Total number of cells in mesh block1 in *x*y*z* direction
1	0.21	1.125	36 × 12 × 30	101× 15× 34
2	0.037	2.25	15 ×6 ×24	51× 8× 17

Table 3. NRMSE values in predicting of the free surface profile (validation with results of Lobovsky et al. 2014)

	Model 1				Model 2			
Time (s)	0.45	0.37	0.28	0.16	0.45	0.37	0.28	0.16
NRMSE	0.05450	0.109	0.0294	0.0375	0.0565	0.0995	0.0262	0.0385

The running time was about six times when the mesh resolution in the model validations was about two times (Table 2). Moreover, the lowest model accuracy was observed at t = 0.37s (Table 3).

The NRMSE values below 0.1 mean that the model has the highest accuracy in predicting the height of the free surface (Table 3). For Models 1 and 2, the highest and lowest accuracy of the model in reproducing the wave evolution across the downstream was at t = 0.28s and t=0.37s, respectively. The NRMSE values at these time points were 3% and 10%, respectively. The possible reason for the decrease in model accuracy at t = 0.37 was the rapid increase in the velocity of the reservoir, which was evident in the numerical results (Fig. 5h-5j). In fact, the model overestimated the velocity of the reservoir release. In the experimental results, on the other hand, the water column had collapsed and the wave propagated slowly downstream because of the resistance created by the removal of the sluice gate and the potential energy. However, in the other cases, the prediction error was less than 6%. Thus, the performance of the model in predicting the profile of the free surface was remarkable. The model was validated using the mesh resolution in three cases with the mean cell size d_0 = 1.25cm, 2.5cm and 3.75cm and the turbulence models of RANS and LES at three time points after the dam break of t = 0.16s, 0.28s, 0.37s (Fig. 5). The initial depth of water in the reservoir H_{w0} was 0.3 m at the initial point of the reservoir x = 0. The length of the prismatic laboratory channel was 1.1 m. The performance of the model did not change dramatically at a mesh resolution of d_0 = 1.25 cm compared to d_0 = 2.5 cm. However, the accuracy of the model in predicting the profile of the free surface was significantly lower at a mesh resolution of d_0 = 3.75 cm (Figs. 5a to 5j). There was no significant difference in the prediction of the free surface profile between the turbulence models of RANS and LES. The reason may have been the simple geometry of the downstream channel and the uniform evolution of the dam-break wave (Fig. 5k-5t).

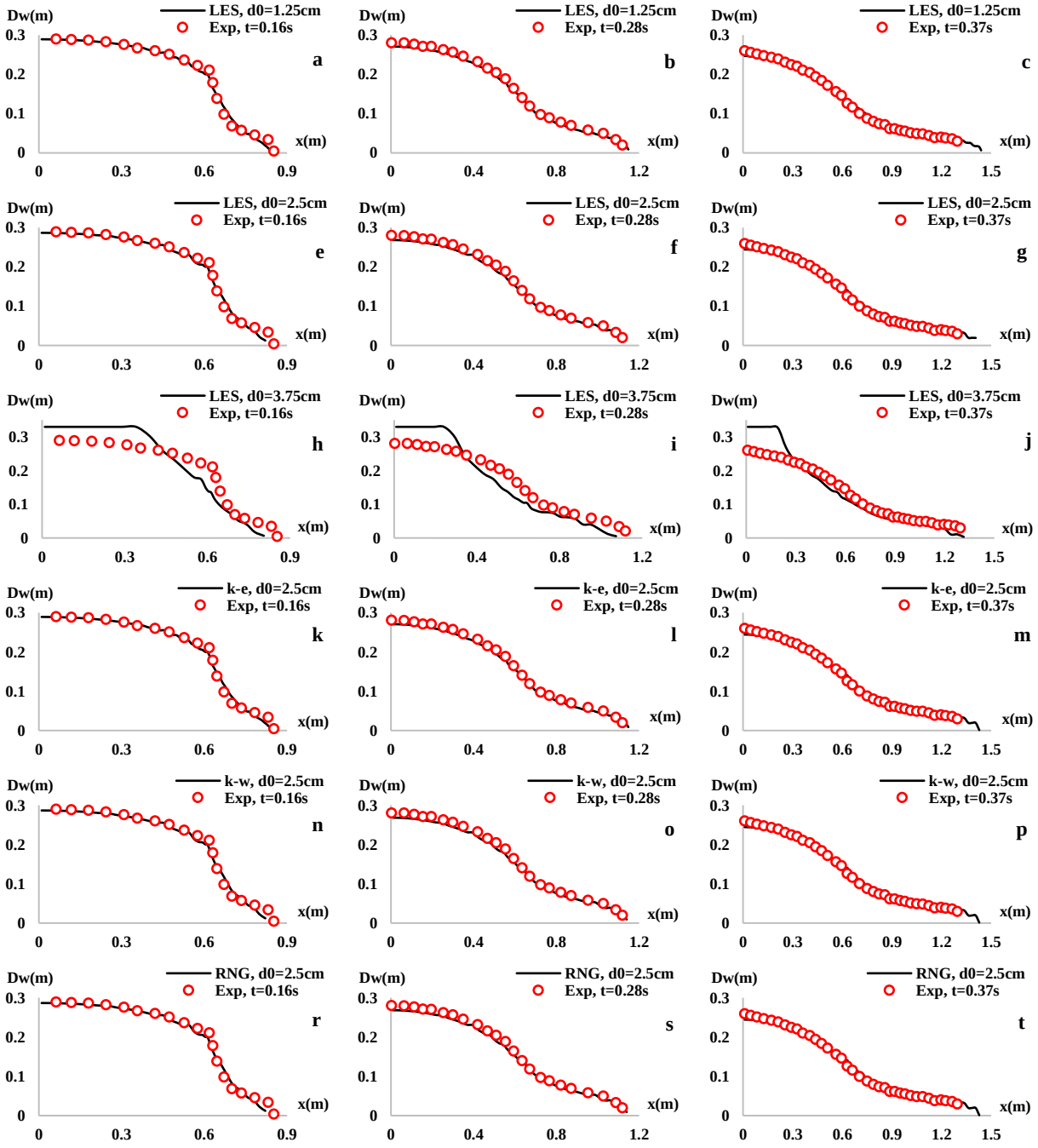

Figure 5. The free surface profile evolution in the experimental (Lobovsky et al. 2014) and the numerical results, (a-j) the sensitivity analysis on the mesh resolution and on the turbulence models (k-t)

Table 4. Dam-break simulation features in triangular (T1) and invert-triangular (T2) models

Model	Total number of cells	Mesh cells mean diameter (cm)	Run time (h)	Mean fluid loss during 10s of simulation (10^{-3} m^3)	Number of mesh blocks
T1	1823595	1.975	1.46	5.76	4
T2	1823595	1.975	2.40	5.42	4

In the present study, the evolution of the dam break wave was reproduced with over 1.8 million cells, and the runtime was significantly higher for the reversed arrangement (T2) compared to the T1 model. The possible reason was the increased resistance to dam break wave evolution caused by the first row of obstacles (Fig. 1 and Table 4).

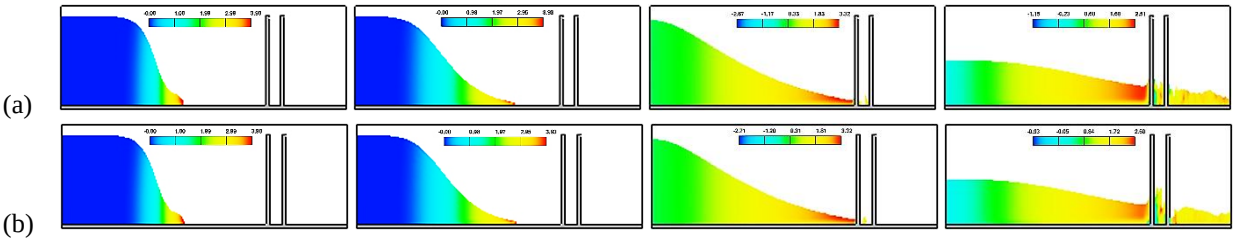

Figure 6. Development of the free surface of the dam breach across the downstream channel (a) model T1 and (b) model T2. The profiles shown in the central axis of the channel. (H/V) scale: (1.5/4)

The development of the dam break waves occurred in five distinct phases: (i) wave formation in the initial stage, (ii) wave development with high velocity over the downstream channel before hitting the obstacles, (iii) wave reflection at the obstacles and slowing down of the flow, (iv) crossing the obstacles with fluctuations of the free surface, (v) attenuating of the wave over the downstream channel (Fig. 6).

The dam break flow was two-dimensional in phase (i), with a steep gradient of free surface in the dam area and a smooth curve in the reservoir. Thereafter, the free surface gradient at the wave front decreased while the wave accelerated in phase (ii). In this phase, the transitional flow developed. Accordingly, the free surface was smoothed throughout the channel in phase (iii). The height of the free surface was reduced by the time evolution of the dam break flow during phases (i-v) throughout the channel. In phases (iii-v), the flow had a three-dimensional character around the obstacles after impact. It is worth noting that the height of the wave runup over the obstacles was higher in model T2 than in model T1 (Fig. 6). The results were consistent with those of Ozmen-Cagatay and Kocaman (2012), Kocaman and Ozmen-Cagatay (2012). However, they did not report the effect of the arrangement of the obstacles on the run-up of the flow over the obstacles.

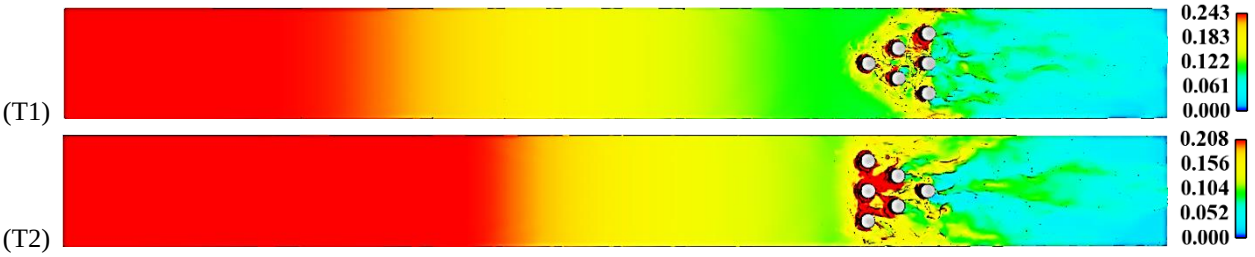

Figure 7. The wave evolution acoss the channel in models T1 and T2 at t = 4s. The color scale shows the free surface height (m)

The reservoir was emptied faster in model T1 than in model T2. In addition, wave runup over the obstacles was higher in model T2 than in T1. The flow separation was significant downstream of the second and third rows of obstacles in model T1, but only around the third row of obstacles in model T2. Accordingly, the superposition of transverse waves downstream of the third row of obstacles was observed in both models (Fig. 7). The result is consistent with that of Soares-Frazao and Zech (2007, 2008). However, they did not investigate the effect of aligned obstacles in the downstream channel.

Wave runup over the first row of obstacles was approximately the same in both models, but not in the third row at t = 2s and t = 4s. In addition, free surface fluctuations developed downstream at t = 4s. However, dam flow was dominant in the fluctuations upstream of the obstacles. The height of the run-up was reduced by wave development over the downstream channel. A mixed flow regime was observed around the obstacles (Fig. 8).

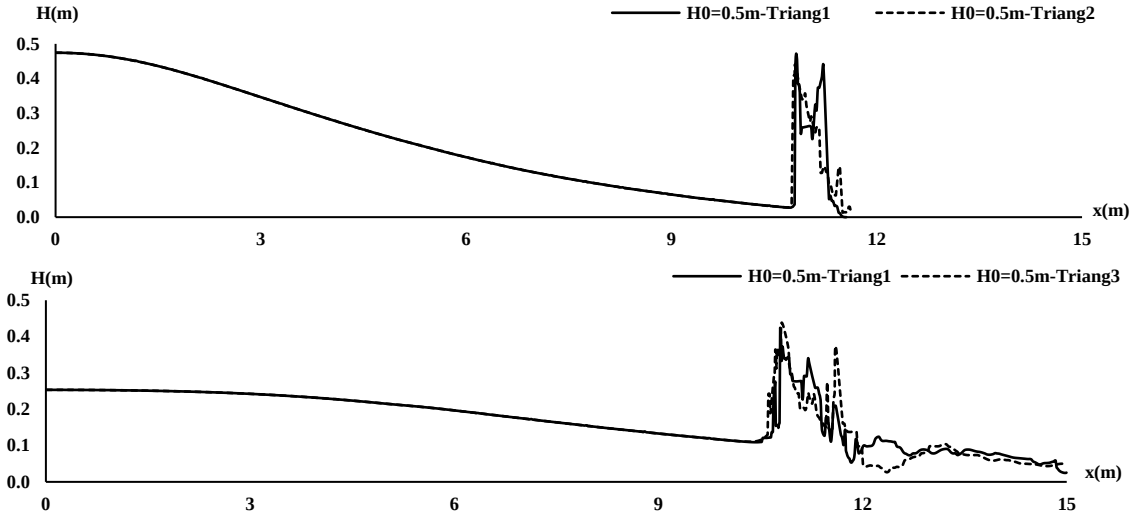

Figure 8. Dam-break free surface profiles in models T1 nad T2 at t =2s and t = 4s (central axis of channel)

In T1 and T2, there is no difference in the leading distance of the dam break wave. Thus, the arrangement of the obstacles is not a significant factor in the distance of the wave development. The result agrees with Ritter's analytical solution for wave dynamics over the fixed bed (Nsom et al. 2000-2019).

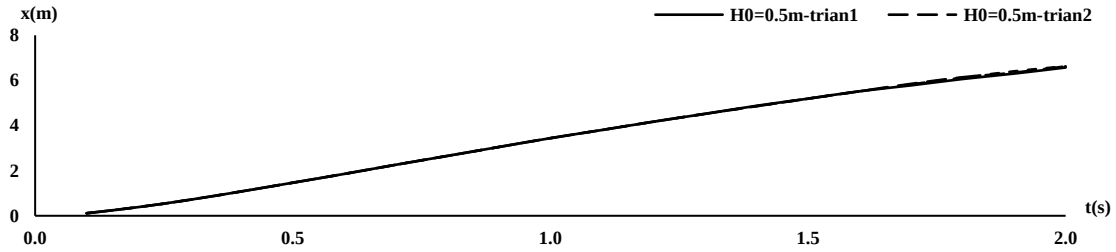

Figure 9. Advancing distance of the dam-break wave in models T1 and T2

The wave front propagating along the downstream channel during a dam failure in length x and time t had an upward trend in both models in triangular and inverted triangular configurations. It is worth noting that the arrangement of the obstacles did not significantly affect the distance of wave development during time (Fig. 9).

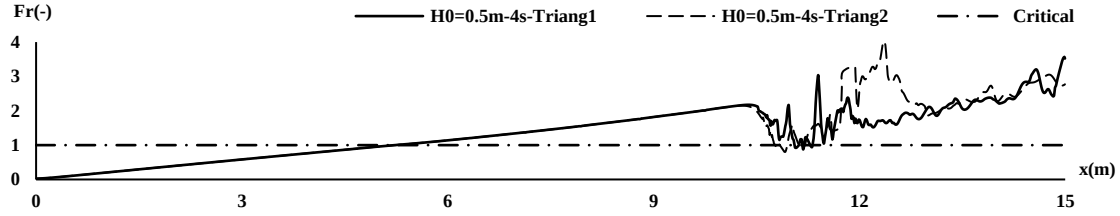

Figure 10. Froude number values across the channel in models T1 and T2

The Froude number is a criterion for the flow regime in an open channel. The unit value signifies the transitional flow, while the supercritical flow is formed when the Froude number value exceeds unity. In contrast, subcritical flow is formed when the Froude number is below unity. The fluctuations of the Froude number reflect the instantaneous change in the profile of the free surface and, consequently, in the depth-averaged velocity of the flow. As can be seen in Figure 10, the plots were converged upstream from the starting point of the channel at x = 0 to x = 10.5 m near the obstacles. The direct dashed line shows the critical flow with Fr = 1. In fact, the dam break wave propagated rapidly in the downstream channel while the Fr values increased from zero at x =0 (the initial point of the reservoir) to about Fr = 2 at x = 10.5m near the obstacles. Thereafter, the value decreased to one by the first row of obstacles in both the triangular T1 and inverted triangular T2 models. However, the peak Froude number in model T2 (Fr = 3.7) was higher than the value in model T1 (Fr = 2.8) around the obstacles. The increasing trend continued downstream of the obstacles and through the flow exiting the outlet. The values of Froud number were changed with increasing tendency when they exceeded the critical value around the dam site. In fact, the flow regime was changed from subcritical in the reservoir to supercritical in the downstream channel. It is noteworthy that another change occurred in the first row of the obstacles where the Froude number values decrease while reaching the critical value with significant fluctuations. The main reason for the fluctuations is the formation of cross currents around the obstacles and the rapid change in depth-averaged velocity at this location over time. The Froude number values are significantly higher in model T2 than in model T1 around the obstacles in rows 2 and 3.

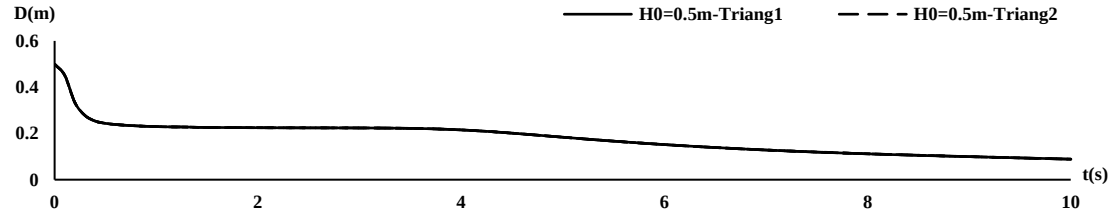

Figure 11. Temporal variation of the dam-break outflow depth in models T1 and T2

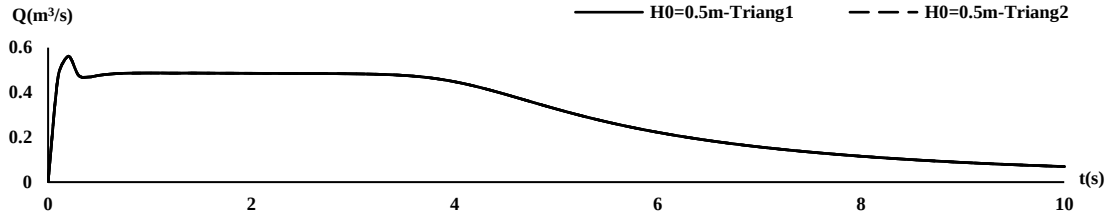

Figure 12. Dam-break outflow hydrograph in the dam site in models T1 and T2

The arrangement of the obstacles has no effect on the temporal variation of the discharge depth and hydrograph in the dam area (Figs. 11 and 12). This is because the drag effects of the obstacles do not affect the reservoir, considering how far the obstacles are from the reservoir. The reservoir is emptied in the initial stage rapidly. Therefore, the steep slope is observed in the initial stage. The duration of rapid emptying of the reservoir is of the same order of magnitude as the instantaneous collapse of the water column at the dam site (Fig. 11).

According to Fig. 12, the outflow hydrograph also does not change with the obstacle's arrangement. The rising limb of the hydrograph has a steep gradient, while in the initial stage it rises to the peak value Qpeak. After that, it decreases slightly to the equilibrium flow rate Qe. The equilibrium flow rate is constant in the middle stage and decreases in the middle to last stages due to wave damping (Fig. 12). The results are consistent with those of Fraccarollo and Toro (1995) and Khoshkonesh et al. (2019).

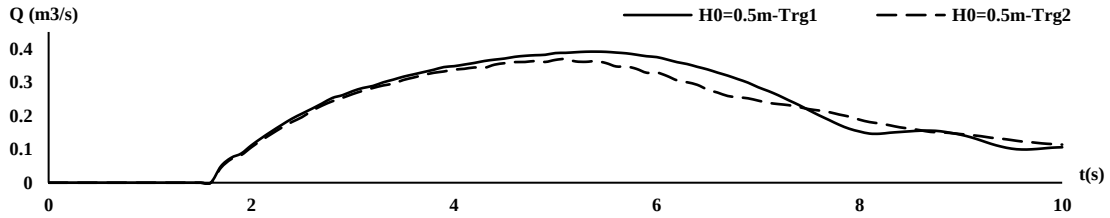

Figure 13. Dam-break inflow hydrograph in the obstacles' place in models T1 and T2

The inflow hydrograph has a lower value in model T2 than in T1 because the reservoir is emptied faster in model T1. However, the models converge during the last stages. Therefore, placement of obstacles may affect the inflow hydrograph in the downstream channel. The peak inflow is larger in model T1 than in T2. Accordingly, the outflow of the dam breach is discharged more when it flows through model T1 (Fig. 13).

Flow in a dam breach is three-dimensional, and the components of flow velocity u, v, and w change in each section around the obstacles. As can be seen in Figure 14, the sign of the velocity changes in different directions around the obstacles. However, the horizontal component *u* has a positive sign in the y-direction. The velocity peak is about $u = 0.6$m/s in the horizontal direction, while the minimum value over the obstacle body is zero. The positive values are the horizontal velocity in the dominant downstream direction. The negative values are negligible. This is because the flow in the horizontal direction did not pass over the upstream obstacles. Moreover, the sign of the transverse velocity in the y-direction of the channel around the obstacles changed between $v = -1$m/s and 0.8m/s. In fact, the flow evolution was dominant on the left side of the transverse direction. Moreover, the vertical velocity values were higher than the horizontal and transverse velocity values. The peak values changed between $w = -1.5$m/s and $w = 1.7$m/s in both upward and downward directions. The horizontal velocity component *u* is zero above the obstacles, but the velocity values increase and then decrease between the obstacles. In fact, the stagnation points form upstream above the obstacles. It is clear that the variations in flow velocity are larger in model T2 than in T1 because the drag effects of the obstacles in the first and second rows are larger in model T2 than in T1. The highest velocity values are observed in the vertical direction z, where the sign of the velocity changes from negative to positive. This is due to the fact that the flow develops in opposite directions after hitting the obstacles. Moreover, the value of the flow velocity between the obstacles and the sidewalls is negligible. The reason could be the small distance between the obstacles and the sidewalls and the dominance of the wall effects on the flow evolution. In fact, the distribution of the flow in different directions during a dam failure leads to a reduction of the flow energy when passing through the obstacles and the sidewalls (Fig. 14).

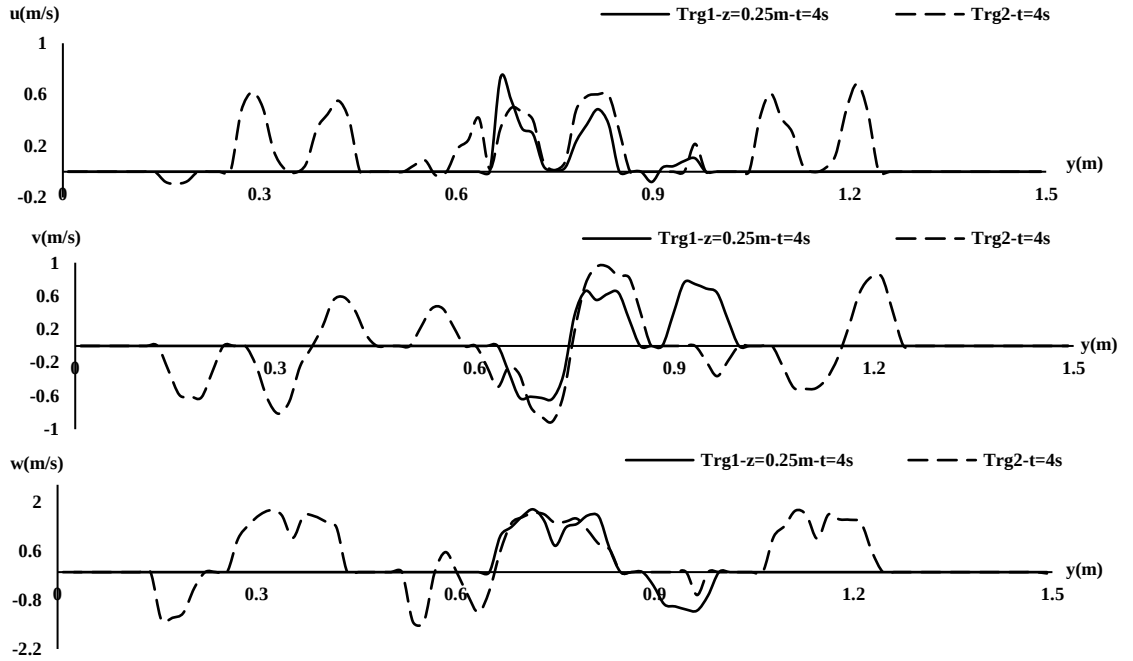

Figure 14. The velocity transverse profiles in three dimensions of Cartesian coordinates in models T1 and T2 at t = 4s (Input of mesh block 3)

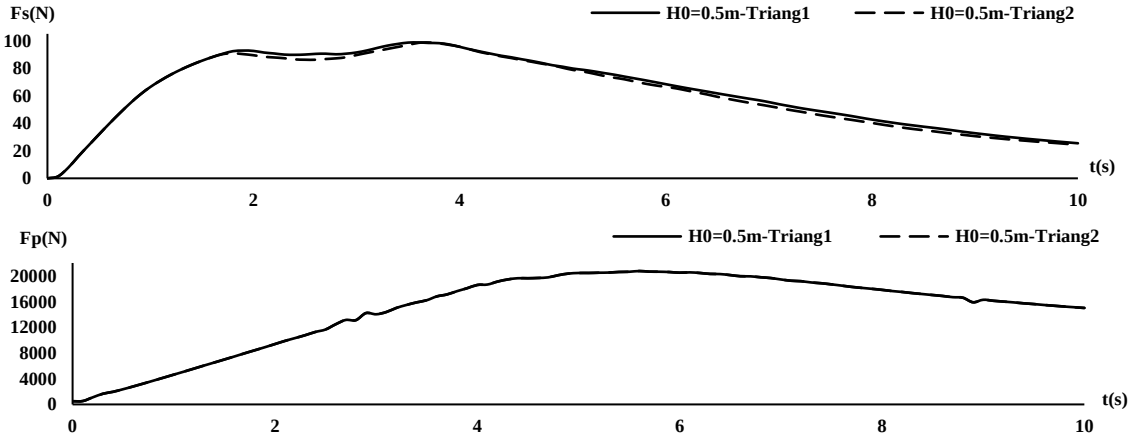

Figure 15. The resultants of pressure and shearing forces within the reservoir in models T1 and T2

The pressure and shear forces act on the reservoir in different normal and tangential directions because of collapsing the stationary water column in the reservoir when the dam breaks. The shear force values increase in both horizontal and normal directions in the initial stage due to the rapid development of the free surface. Shear force F_s values increased from zero to about 90 N during t = 2s after dam failure. The increase was due to the rapid development of the wave front in the horizontal direction in the downstream channel. However, the shear force increased with a slight slope to about 100 N during t = 2s to t = 4s. This was due to the propagation of a weak negative wave over the reservoir, which was opposite to the dominant wave propagation downstream. Thereafter, the shear force values decreased to about 20 N at t = 10s because the flow depth was reduced by the exit of the dam-break flow from the outlet and wave damping. The resultant pressure force in the reservoir was increased from zero at t = 0 to about 20 KN at t = 5s. Thereafter, the value was constant during t = 5s to t = 6.5s. Wave propagation across the downstream channel decreased the pressure force values with a slight gradient to about 15 KN. The pressure force values were significantly higher than the shear force because of water column weight. These values increase with a steep gradient from the first to the middle stage. This is due to the delay in outflow from the reservoir during dam failure and the significant difference between the momentum of the wave front and the static water in the reservoir. However, the values for the pressure force decrease with a slight gradient during the middle to last stages. It is clear that the highest resultant pressure force occurs during the middle stage when the reservoir was most depleted (Fig. 15).

4. Conclusion

The instantaneous wave development during a dam breach was modelled using a CFD package, while the effects of the downstream obstacle were investigated in a numerical approach. The model showed high accuracy in predicting the evolution of the free surface of the dam breach, but overestimated the outflow hydrographs of the reservoir. The performance of the model was highly dependent on the mesh resolution, while the fluid loss was negligible. The results showed that the arrangement of the obstacles played a significant role in the free surface elevation,

reservoir discharge rate, three-dimensional flow velocity, and flow regime around the obstacles. However, there was no specified relationship between the arrangement and the wave development distance and the resulting forces acting on the reservoir.

5. References

1. Ahadiyan, J., Bahmanpouri, F., Adeli, A., Gualtieri, C., & Khoshkonesh, A. (2022). Riprap effect on hydraulic fracturing process of cohesive and non-cohesive protective levees. Water Resources Management, https://doi.org/10.1007/s11269-021-03044-6.
2. Aureli, F., Dazzi, S., Maranzoni, A., Mignosa, P., & Vacondio, R. (2015). Experimental and numerical evaluation of the force due to the impact of a dam-break wave on a structure. Advances in Water Resources, 76, 29–42. https://doi.org/10.1016/j.advwatres.2014.11.009
3. Azimi, H., Heydari, M., & Shabanlou, S. (2018). Numerical simulation of the effects of downstream obstacles on malpasset dam break pattern. In Journal of Applied Research in Water and Wastewater (Vol. 10, Issue 2).
4. Bahmanpouri, F., Daliri, M., Khoshkonesh, A., Montazeri Namin, M., & Buccino, M. (2021). Bed compaction effect on dam break flow over erodible bed; experimental and numerical modeling. Journal of Hydrology, 594. https://doi.org/10.1016/j.jhydrol.2020.125645
5. English, A., Domínguez, J. M., Vacondio, R., Crespo, A. J. C., Stansby, P. K., Lind, S. J., Chiapponi, L., & Gómez-Gesteira, M. (2021). Modified dynamic boundary conditions (mDBC) for general-purpose smoothed particle hydrodynamics (SPH): application to tank sloshing, dam break and fish pass problems. Computational Particle Mechanics. https://doi.org/10.1007/s40571-021-00403-3
6. Fan, J. hui, Galoie, M., & Motamedi, A. (2020). Mitigation of the amplitude and celerity of dam break shock wave using combination of groyne and vertical pier. Journal of Mountain Science, 17(6), 1452–1461. https://doi.org/10.1007/s11629-019-5897-6
7. Flow Science (2012) Flow-3D user manual. Flow Science Ltd
8. Fraccarollo, L., & Toro, E. F. (n.d.). Experimental and numerical assessment of the shallow water model for two-dimensional dam-break type problems Experimental and numerical assessment of the shallow water model for two-dimensional dam-break type problems Evaluation expérimentale et numérique. Journal of Hydraulic Engineering-Asce, July 2012, 37–41.
9. Gu, S., Zheng, X., Ren, L., Xie, H., Huang, Y., Wei, J., & Shao, S. (2017). SWE-SPHysics simulation of dam break flows at South-Gate Gorges Reservoir. Water (Switzerland), 9(6). https://doi.org/10.3390/w9060387
10. Hänsch, S., Lucas, D., Höhne, T., & Krepper, E. (2014). Application of a new concept for multi-scale interfacial structures to the dam-break case with an obstacle. Nuclear Engineering and Design, 279, 171–181. https://doi.org/10.1016/j.nucengdes.2014.02.006
11. Hirt, C. W., & Nichols, B. D. (1981). Volume of fluid (VOF) method for the dynamics of free boundaries. Journal of Computational Physics, 39(1), 201–225. https://doi.org/10.1016/0021-9991(81)90145-5
12. Issakhov, A., & Imanberdiyeva, M. (2019). International Journal of Heat and Mass Transfer Numerical simulation of the movement of water surface of dam break flow by VOF methods for various obstacles. International Journal of Heat and Mass Transfer, 136, 1030–1051. https://doi.org/10.1016/j.ijheatmasstransfer.2019.03.034
13. Issakhov, A., & Zhandaulet, Y. (2020). Numerical Simulation of Dam Break Waves on Movable Beds for Various Forms of the Obstacle by VOF Method. Water Resources Management, 34(8), 2269–2289. https://doi.org/10.1007/s11269-019-02480-9
14. Issakhov, A., Zhandaulet, Y., & Nogaeva, A. (2018). Numerical simulation of dam break flow for various forms of the obstacle by VOF method. International Journal of Multiphase Flow, 109, 191–206. https://doi.org/10.1016/j.ijmultiphaseflow.2018.08.003
15. Khoshkonesh, A., Nsom, B., Bahmanpouri, F., Dehrashid, F. A., & Adeli, A. (2021). Numerical Study of the Dynamics and Structure of a Partial Dam-Break Flow Using the VOF Method. Water Resources Management, 35(5), 1513–1528. https://doi.org/10.1007/s11269-021-02799-2
16. Khoshkonesh, A., Nsom, B., Gohari, S., & Banejad, H. (2019). A comprehensive study on dam-break flow over dry and wet beds. Ocean Engineering, 188. https://doi.org/10.1016/j.oceaneng.2019.106279
17. Kocaman, S., & Güzel, H. (2011). Numerical and Experimental Investigation of Dam-Break Wave on a Single Building Situated Downstream. May, 19–21.
18. Kocaman, S., & Ozmen-Cagatay, H. (2012). The effect of lateral channel contraction on dam break flows: Laboratory experiment. Journal of Hydrology, 432–433, 145–153. https://doi.org/10.1016/j.jhydrol.2012.02.035
19. Liu H, Liu H, Guo L, Senxun LU (2017) Experimental study on the dam-break hydrographs at the gate Location. J Ocean Univ China 16(4):697–702
20. Lobovský, L., Botia-Vera, E., Castellana, F., Mas-Soler, J., & Souto-Iglesias, A. (2014). Experimental investigation of dynamic pressure loads during dam break. Journal of Fluids and Structures, 48, 407–434. https://doi.org/10.1016/j.jfluidstructs.2014.03.009
21. Nsom, B., Debiane, K., & Piau, J. M. (2000). Bed slope effect on the dam break problem. Journal of Hydraulic Research, 38(6), 459–464. https://doi.org/10.1080/00221680009498299
22. Nsom, B., Ramifidisoa, L., Latrache, N., & Farzaneh, G. (2019). Linear stability of shear-thinning fluid down an inclined plane. Journal of Molecular Liquids, 227, 1036–1046. https://doi.org/10.1016/j.molliq.2018.12.059
23. Nsom, B., Ravelo, B., & Ndong, W. (2008). Flow Regimes in Horizontal Viscous Dam-Break Flow of Clayous Mud Abstract : WSEAS TRANSACTIONS on FLUID MECHANICS, 18(4), 4–6.
24. Oertel, M., & Bung, D. B. (2012). Initial stage of two-dimensional dam-break waves: Laboratory versus VOF. Journal of Hydraulic Research, 50(1), 89–97. https://doi.org/10.1080/00221686.2011.639981
25. Ozmen-Cagatay, H., & Kocaman, S. (2010). Dam-break flows during initial stage using SWE and RANS approaches. Journal of Hydraulic Research, 48(5), 603–611. https://doi.org/10.1080/00221686.2010.507342
26. Ozmen-Cagatay, H., & Kocaman, S. (2012). Investigation of dam-break flow over abruptly contracting channel with trapezoidal-shaped lateral obstacles. Journal of Fluids Engineering, Transactions of the ASME, 134(8). https://doi.org/10.1115/1.4007154
27. Saghi, H., & Lakzian, E. (2019). Effects of using obstacles on the dam-break flow based on entropy generation analysis. European Physical Journal Plus, 134(5). https://doi.org/10.1140/epjp/i2019-12592-3
28. Soares-Frazão, S., & Zech, Y. (2007). Experimental study of dam-break flow against an isolated obstacle. Journal of Hydraulic Research, 45(sup1), 27–36. https://doi.org/10.1080/00221686.2007.9521830
29. Soares-frazão, S., & Zech, Y. (2008). Dam-break flow through an idealised city Dam-break flow through an idealised city Onde de rupture de barrage à travers une ville idéalisée. Journal of Hydraulic Research, 46(5), 648–658. https://doi.org/10.3826/jhr.2008.3164
30. Wu, J. S., Zhang, H., Yang, R., Dalrymple, R. A., & Hérault, A. (2013). Numerical modeling of dam-break flood through intricate city layouts including underground spaces using GPU-based SPH method. Journal of Hydrodynamics, 25(6), 818–828. https://doi.org/10.1016/S1001-6058(13)60429-1
31. Yilmaz, O., Korobkin, A., & Iafrati, A. (2013). The initial stage of dam-break flow of two immiscible fluids. Linear analysis of global flow. Applied Ocean Research, 42, 60–69. https://doi.org/10.1016/j.apor.2013.04.003
32. Yilmaz, A., Dal, K., Demirci, M., & Kocaman, S. (2017). Numerical Investigation of Dam-Break Flowovera Bottom Obstacle Using Eulerian Finite Element Method. International Journal of Advanced Engineering Research and Science, 4(12), 203–208. https://doi.org/10.22161/ijaers.4.12.30
33. Yu, C. H., Wen, H. L., Gu, Z. H., & An, R. D. (2019). Numerical simulation of dam-break flow impacting a stationary obstacle by a CLSVOF/IB method. Communications in Nonlinear Science and Numerical Simulation, 79. https://doi.org/10.1016/j.cnsns.2019.104934